Mechanistic and Electronic Insights into Efficient Carbon Dioxide Reduction Driven by Visible Light Using a Coordination Polymer

Tsuji, Yuta
Faculty of Engineering Sciences, Kyushu University

Yamamoto, Sayoko
Faculty of Engineering Sciences, Kyushu University

Kamakura, Yoshinobu
Department of Chemistry, School of Science, Tokyo Institute of Technology

Suppaso, Chomponoot
Department of Chemistry, School of Science, Tokyo Institute of Technology

他

出版情報：ACS Applied Energy Materials. 7 (10), pp.4472-4483, 2024-05-14. American Chemical Society (ACS)
バージョン：

Mechanistic and Electronic Insights into Efficient Carbon Dioxide Reduction Driven by Visible Light Using a Coordination Polymer

Yuta Tsuji,[1] Sayoko Yamamoto,[1] Yoshinobu Kamakura,[2] Chomponoot Suppaso,[2] Daisuke Tanaka,[3*] Kazuhiko Maeda[2,4*]*

1. Faculty of Engineering Sciences, Kyushu University, Kasuga, Fukuoka 816-8580, Japan.

2. Department of Chemistry, School of Science, Tokyo Institute of Technology, Meguro-ku, Tokyo 152-8550, Japan.

3. Department of Chemistry, School of Science, Kwansei Gakuin University, Sanda, Hyogo 669-1337, Japan.

4. Living Systems Materialogy (LiSM) Research Group, International Research Frontiers Initiative (IRFI), Tokyo Institute of Technology, 4259 Nagatsuta-cho, Midori-ku, Yokohama, Kanagawa 226-8502, Japan.

ABSTRACT

In this study, a comprehensive theoretical analysis was undertaken to elucidate the remarkably efficient conversion of CO_2 into $HCOO^-$ employing a coordination polymer (CP) featuring Pb-S bonds, namely $[Pb(tadt)]_n$ (where tadt stands for 1,3,4-thiadiazole-2,5-dithiolate), referred to as KGF-9. The catalytic activity of this visible-light responsive solid photocatalyst has been carefully compared with that of PbS, a typical compound that also contains the Pb-S bond. The former shows a very high catalytic activity, while the latter shows almost no activity. The photoreduction process of CO_2 on the KGF-9 surface was analyzed in detail using periodic density functional theory calculations. The reduced catalyst surface was modeled as a hydrogenated surface. The reaction at the active center of a formate dehydrogenase provides an interesting contrast, suggesting that the S-H group plays an important role in the conversion of CO_2 to $HCOO^-$. However, the S-H group on the reduced PbS surface does not facilitate the conversion to the same extent as KGF-9. This is because the electrons supplied to CO_2 on the PbS surface come from deep within the solid, whereas on KGF-9, they come from the top surface. This difference is due to differences in the electronic structure of the S-H bond, band gap, and valence band maximum position between the two surfaces, accounting for the marked difference in their catalytic activity. These insights are consistent with experimental and computational results on the thermodynamic and kinetic characteristics of the CO_2 reduction reaction of KGF-9 and PbS, and provide guidance for the design of CO_2 photoreduction catalysts.

KEYWORDS: artificial photosynthesis, photocatalyst, CO_2 reduction, CO_2 adsorption, coordination polymer, DFT calculation, orbital interaction

TOC GRAPHICS

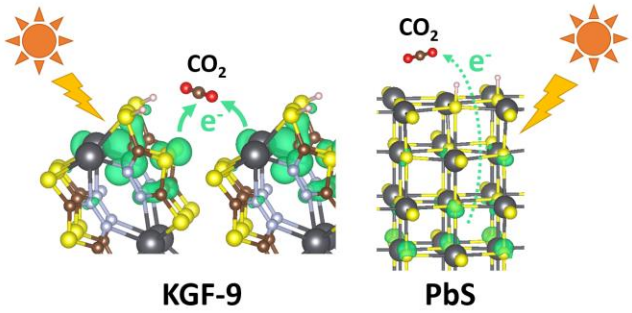

Introduction

Coordination polymers (CPs) are materials that combine inorganic and organic components in which metal ions and clusters are bound by organic ligands.[1] CPs are particularly attractive as photocatalysts for CO_2 conversion because the diverse coordination chemistry derived from the combination of metal ions and organic ligands, efficient sunlight absorption, and highly dispersed active sites can be used to integrate light-harvesting and catalytic components for artificial photosynthesis.[2,3] Despite these excellent properties of CP, there is still much to be studied regarding the catalytic mechanism of CP, especially with respect to structural design strategies.[4] Researchers are trying to understand the multi-electron reactions in CP-based catalysts and the influence of the organic environment surrounding the metal ions on the catalytic performance; further theoretical studies are crucial to understand the photocatalytic process using CP materials and to develop a basic framework for the design of CP-based catalysts.[5] This, in turn, will lead to the development of a fundamental paradigm for the design of CP-based catalysts.

In the existing literature, there are few theoretical studies that have investigated CO_2 reduction by CP photocatalysts using methods such as density functional theory (DFT).[6,7,8] These studies often use monomer units as models and provide insight into stability, electron transfer properties, band alignment, and catalytic cycle. However, CP is a crystalline material and photocatalysis occurs primarily at the surface. It would be difficult to determine the effect of CP surface morphology on catalysis using calculations based on the monomer model. Also, the electronic state of the catalytically active site may be affected by that of the neighboring repeating unit. Understanding the difference between bulk and surface structures is critical. In this study, the CP surface is approximated by a slab model and the mechanism of CO_2 reduction by a CP photocatalyst is investigated using a periodic DFT method.

Some of the coauthors of this paper synthesized KGF-9, a highly crystalline CP with a three-dimensional structure containing a two-dimensional Pb-S skeleton (Scheme 1), whose structure was confirmed by single-crystal X-ray diffraction.[9] The phase purity of the synthesized KGF-9 was confirmed by CHN elemental analysis and powder X-ray diffraction. It was shown that KGF-9 efficiently absorbs visible light up to 500 nm. Time-resolved microwave conductivity and direct-current photoconductivity measurements were performed on KGF-9,[9] and the results of those experiments strongly suggested that carriers were generated by photoirradiation. In addition to such interesting structural and optical properties, KGF-9 was shown to function as a photocatalyst, with a selectivity of >99% for the conversion of CO_2 to $HCOO^-$ and an apparent quantum yield at 400 nm is 2.6%.[10] To evaluate the photochemical stability of KGF-9 under photocatalytic conditions, powder X-ray diffraction and X-ray photoelectron spectroscopy measurements as well as field-emission scanning electron microscopy observations were performed after the photocatalytic reaction.[10] Based on the results of such experiments, it was shown that KGF-9 generally maintained its skeletal structure under the reaction conditions, although a slight degradation of the surface structure was suggested. Notably, KGF-9 does not require cocatalysts such as noble metals and has active CO_2 reduction sites on its own surface; KGF-9 has Pb(II) as its metal center, but classical Pb-S compounds such as PbS are known not to work as a catalyst. This suggests the significance of the contribution of elements other than Pb in CO_2 reduction by KGF-9. In this paper, we harness insights from a range of scientific disciplines, such as theoretical chemistry, catalytic chemistry, semiconductor physics, and bioinorganic chemistry, to unveil the exceptional catalytic activity of KGF-9 through a comparative analysis with PbS.

Scheme 1. Left: Schematic of the Synthesis of KGF-9 from 1,3,4-Thiadiazole-2,5-Dithiol (H_2tadt). Right: Network Structure Formed by KGF-9 Based on the Pb-S Bond.

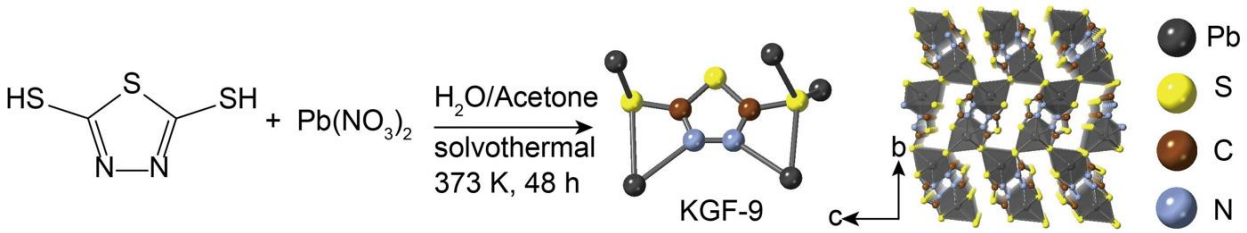

Methods

The crystal structures of KGF-9 and PbS, available from CCDC and ICSD (CCDC 2046612 for KGF-9, ICSD 38293 for PbS), were fully optimized using the Vienna ab initio simulation package (VASP) 5.4.4[11,12] (see Figures 1a and 1b). The PBE functional[13] was used with a plane-wave basis set and the PAW method.[14] The cutoff energy was set to 500 eV. The convergence criterion for the electronic self-consistent field (SCF) loop was set to 1.0×10^{-5} eV. Both the atomic positions and cell parameters were fully optimized until the forces on all the atoms became less than 0.01 eV/Å. The Γ-centered k-point meshes with a k spacing of $2\pi \times 0.05$ Å^{-1} were employed for sampling the Brillouin zone. Grimme's D3 dispersion correction formalism with Becke–Johnson damping[15] was adopted. Optimized structures shown in this paper were drawn by using VESTA.[16] The optimized KGF-9 and PbS lattice constants are compared to those obtained experimentally in Table S1 in the Supporting Information (SI).

Miller indices for typical surfaces of KGF-9 and PbS are reported to be (010) and (100), respectively.[9,17] Based on scanning electron microscopy images, it is reported that KGF-9 forms plate-like crystals.[9] The KGF-9 plate surface consists of a two-dimensional Pb-S coordination

sheet with a Miller index of (010), which is supported by single-crystal XRD measurements.[9] Surface energy calculations reported in the literature indicate that the (100) facet of PbS is the thermodynamically stable surface with the lowest surface energy of the low-index facets.[18] Thus, the KGF-9 and PbS surfaces were approximated by the (010)-(2×1) and (100)-(2×1) slab models, respectively (see Figures 1c and 1d). The results of the validation of these slab model thicknesses are presented in Figures S1 and S2. A 20 Å-thick vacuum layer was placed on the surface. The same functional, dispersion correction, cutoff energy, and SCF tolerance used in the bulk calculations were also used in the slab calculations. A Γ-centered k-point grid with a k spacing of $2\pi \times 0.05$ Å^{-1} ($2 \times 2 \times 1$ k-point grid) was used. In order to reduce computational costs, the convergence conditions for the optimization were relaxed to a threshold of 0.05 eV/Å. The coordinates of all atoms were fully relaxed.

To obtain the transition state (TS) structure, we performed climbing image-nudged elastic band (CI-NEB) calculations.[19,20] The spring constant between adjacent NEB images was set to 5.0 eV/Å^2. The calculation conditions were otherwise identical to those used for the slab calculations. We have performed vibration calculations for the TS structure and found that there is only one imaginary frequency.

To better understand the electronic state of surface bonding, we utilized LOBSTER v4.1.0[21,22] to calculate the crystal orbital Hamilton population (COHP). The crystal orbital bond index (COBI)[23] was calculated to quantify the covalent bond strength of surface bonds. The Bader charge analysis[24,25] was also conducted.

Quantum chemical calculations for discrete molecular systems were performed using the B3LYP functional in conjunction with the 6-31G(d) basis set as implemented in Gaussian 16.[26] A

fragment molecular orbital (FMO) analysis[27] was performed using an extended Hückel program (YAeHMOP)[28] in order to clarify the orbital interaction, and FMO diagrams were drawn using Viewkel.[28]

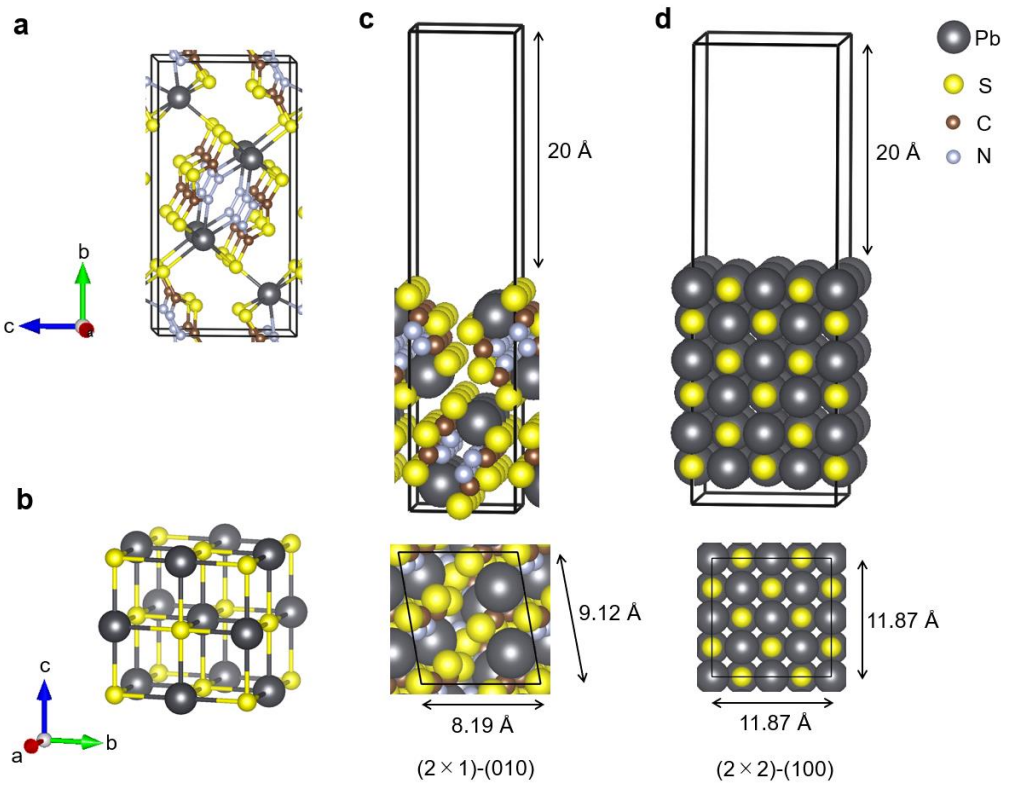

Figure 1. Optimized crystal structures of (a) KGF-9 and (b) PbS. Side and top views of the optimized slab model structures for the (c) KGF-9 (010) and (d) PbS (100) surfaces.

Results and Discussion

A postulated reaction mechanism for CO_2 reduction with KGF-9 is shown in Scheme 2. The reduction of CO_2 presents a significant challenge from both a thermodynamic and kinetic standpoint, as it necessitates the transfer of multiple electrons with substantial energy levels, yielding a diverse range of products. Consequently, it becomes imperative to advance the development of photocatalytic CO_2 reduction systems that can demonstrate elevated levels of activity and product selectivity when subjected to visible light, albeit at the cost of utilizing sacrificial electron donors.[29,30,31] Absorption of visible light produces an electron (e^-)-hole (h^+) pair. Oxidation of the sacrificial agent, 1,3-dimethyl-2-phenyl-2,3-dihydro-1*H*-benzo[*d*]imidazole (BIH), provides two electrons,[32] one of which is used to remove h^+ in the valence band (VB) and the other to reduce KGF-9 (see Supplementary Note 1 in the SI for further discussion). Along with those electrons, a proton is released, which is considered to be adsorbed on the surface of the catalyst. This can be regarded as reductive hydrogenation of the catalyst surface by BIH. Although we have not yet been able to spectroscopically observe the hydrogenated catalyst surface, the validity of the model is confirmed by comparing the results of the first-principles simulation on the reaction with the experimental results.

The diagram in Scheme 2 implies two electrons in the conduction band (CB) per unit cell, which, given the periodicity, corresponds to a state in which a myriad of electrons are present in the CB. Such an accumulation of electrons is expected under steady-state illumination conditions. During the CO_2 reduction reaction, KGF-9 exhibits a dark greenish color (Figure S4a), indicating the accumulation of electrons in the CB. This change could also be evidenced by the increase of absorption from 500 to 800 nm as can be seen from Figure S4b.

Scheme 2. Schematic Energy Diagram for the Reduction of CO_2 and the Oxidation of BIH on the Surface of KGF-9.

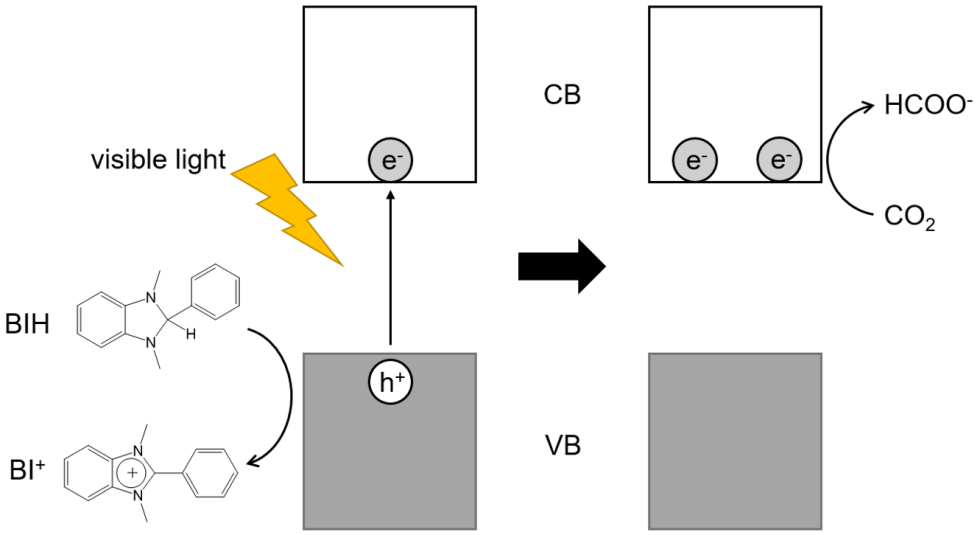

There are several possible methods to calculate the surface of the two-electron reduced KGF-9, including adding hydrogen atoms (each providing one electron), creating anion defects by removing sulfur atoms, and manually adjusting the number of electrons in the unit cell.[33,34,35] These methods may introduce artificial interactions and local relaxation. Therefore, results should be interpreted as representing qualitative trends. In this system, it is reasonable to assume that BIH provides both electrons and protons to the KGF-9 surface and that H is used for CO_2 hydrogenation; given that CO_2 and H co-adsorption is the precursor state for CO_2 hydrogenation, modeling the KGF-9 surface as hydrogenated would most closely resemble the actual system. Models for two-electron reduced surfaces of KGF-9 and PbS with two hydrogen atoms (KGF-9-2H and PbS-2H) were created. For comparison, surface models with only one hydrogen atom introduced, corresponding to a one-electron reduced state, were also considered (KGF-9-1H and

PbS-1H). We investigated the most stable adsorption position of an H atom on the KGF-9 and PbS surfaces, finding that on both surfaces, the most stable state is that in which an S-H bond is formed on the topmost surface (see Supplementary Note 2 in the SI for the details of the model construction). The structures of the reduced surface model thus obtained are shown in Figure 2. DFT calculations for CO_2 photoreduction were performed using these surfaces. Note that the two-electron reduction does not mean that the surface Pb is locally reduced to Pb(0); the results of the Bader charge calculations performed for the KGF-9 and KGF-9-2H surfaces indicate that, moving from the non-reduced surface to the two-electron reduced surface, the average reduction in the positive charge of the top surface Pb is as small as 0.13.

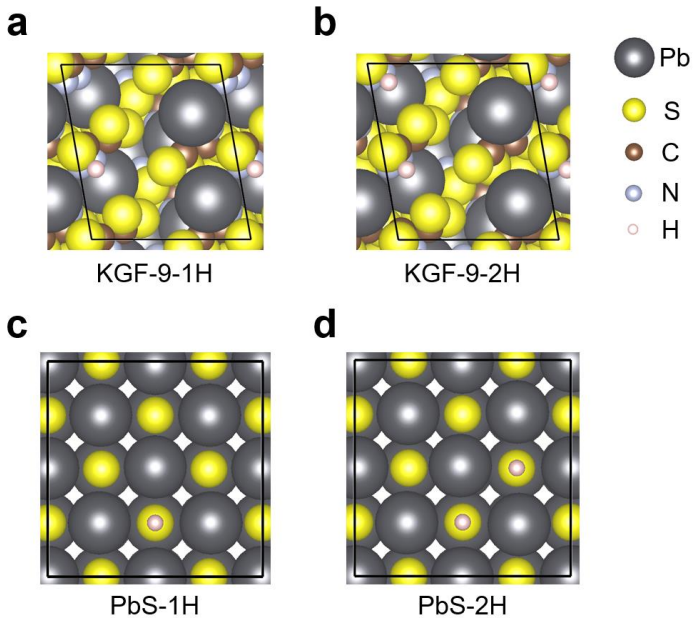

Figure 2. Top views of the surface structures of (a) KGF-9-1H, (b) KGF-9-2H, (c) PbS-1H, and (d) PbS-2H.

Since S-H groups are likely to be present on the surface of hydrogenated KGF-9 and PbS, the involvement of the S-H groups in CO_2 reduction was investigated. Insights were gained from the formate dehydrogenase (FDH) of the sulfate-reducing bacterium *Desulfovibrio desulfuricans*, which catalyzes the reversible oxidation of formate to CO_2, influenced by the availability of formic acid (subsequently formed from the formate) and CO_2 and the production of Mo^{6+} and Mo^{4+} centers (Scheme 3a).[36,37,38] It should be noted, however, that a different mechanism has also been proposed than the one presented here.[39] The FDH enzyme catalyzes not only the oxidation of formate but also the reduction of CO_2; the FDH catalyst undergoes reduction with one proton and two electrons, similar to the reduction of the KGF-9 surface by BIH. Based on the above, the states in the mechanism of CO_2 reduction using S-H groups on the KGF-9 and PbS surfaces were classified into states **1**, **2**, and **3** as shown in Scheme 3b. Note that the adsorption mode of formate in state **3** is shown only schematically. Referring to the literature,[40] several adsorption modes of formate on Pb compounds can be assumed, as shown in Scheme 4. However, as will be shown later, the η^2 mode or μ mode is more stable than the η^1 mode. The surface coordination mode of formate and its likelihood of occurring is better corroborated by experimental observation, ideally by spectroscopic techniques such as IR. However, this is very difficult to do. That is why the help of theoretical studies is needed.

Scheme 3. Schematic of the CO_2 Reduction Reaction Involving the S-H Group in the Active Center of an Enzyme and the Reaction at the Surface with Reference to It.[a]

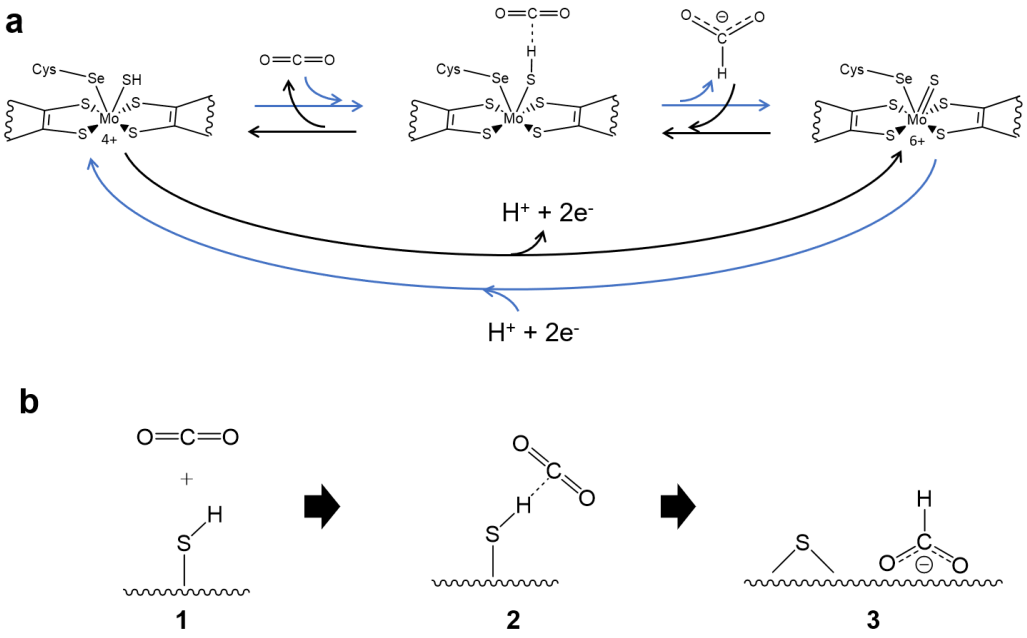

[a](a) Reaction mechanism for FDH-catalyzed formate oxidation (black arrows) and CO_2 reduction (blue arrows). The direction of this reversible reaction depends on the predominant oxidation/reduction state of molybdenum and the presence of formic acid/carbon dioxide. This diagram was drawn with reference to Refs. 36, 37, and 38. (b) CO_2 reduction mechanism by an S-H group on the surfaces of KGF-9 and PbS, drawn based on the mechanism of CO_2 reduction by the FDH catalyst: starting with the catalyst surface and CO_2 separated (**1**), CO_2 is adsorbed on the catalyst surface (**2**), and then the formate produced is adsorbed on the catalyst surface (**3**). The wavy line indicates that the structure beyond it is omitted.

Scheme 4. Schematic Diagram of Possible Adsorption Modes of Formate to Pb Atoms.

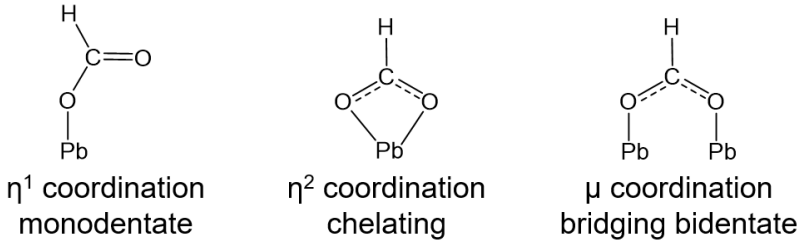

The energy landscape of CO_2 reduction on the KGF-9 and PbS surfaces has been studied for one-electron reduced surfaces and the two-electron reduced. A variety of CO_2 adsorption configurations were considered. The plots of energy for the minimum and maximum energy structures in each state are shown in Figure 3 (what is shown here is a digest version; see Supplementary Note 3 in the SI for details). We found a reaction pathway that destabilizes as the reaction proceeds at the one-electron reduced surfaces, while on the two-electron reduced surfaces the energy continues to decrease as the reaction proceeds. The presence of more stable reaction pathways on the two-electron reduced surfaces highlights the importance of the two-electron reduced surface in the conversion of CO_2 to $HCOO^-$. However, even if one were to consider what would be a three-electron reduced surface, this stabilization trend would not change (Figure S8). This corresponds well with the fact that the conversion of CO_2 to $HCOO^-$ is a two-electron reduction. Furthermore, the reaction in KGF-9-2H is more exothermic than that in PbS-2H, suggesting the higher catalytic activity of KGF-9-2H, in agreement with the experimental results.[10]

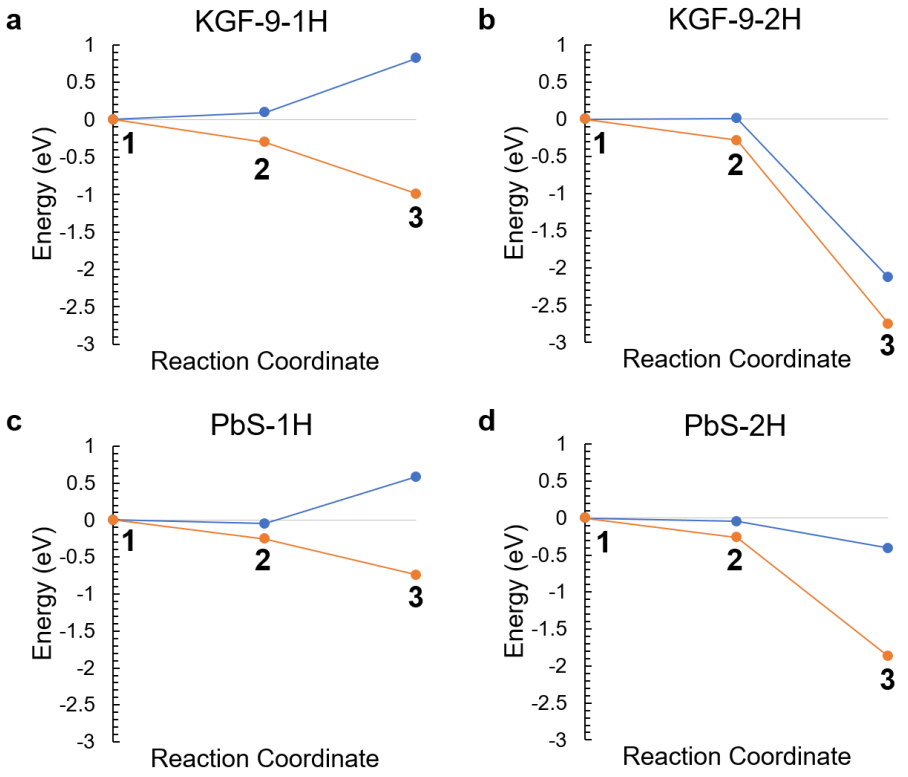

Figure 3. Energy changes of states **1**, **2**, and **3** on (a) KGF-9-1H, (b) KGF-9-2H, (c) PbS-1H, and (d) PbS-2H surfaces. Of the many adsorbed structures found in each state, those with the lowest energy are indicated in orange and those with the highest energy are indicated in blue.

Figure 3 reflects well the thermodynamic aspects of this reaction, but a discussion of the kinetic aspects is also necessary. Among the numerous adsorption configurations, the most stable configuration was selected for further analysis. The TS connecting states **2** and **3** was identified on the two-electron reduced surfaces as shown in Figure 4a. Comparing the energy diagrams, the conversion of CO_2 to $HCOO^-$ has almost no barrier on the KGF-9-2H surface, while an 8-fold higher activation barrier of 0.31 eV was observed on the PbS-2H surface. Although an essentially equivalent energy diagram was obtained in calculations taking into account spin-orbit couplings[41]

(Figure S10), only the activation energy on PbS-2H increased slightly from 0.31 eV to 0.46 eV. Figures 4b and 4c show the structural details of the reaction. Note that these structures were obtained by re-optimization during the CI-NEB calculation process. They do not exactly match the most stable structure of each state shown in Figure S7. For example, the most stable structure in state **2** shown in Figure S7d was found to be unsuitable as the initial structure for the H-transfer reaction, so the structure shown in Figure 4c was adopted. The energy difference between them is about 0.05 eV.

On KGF-9-2H, CO_2 is contained in a surface recess, suggesting that CO_2 adsorption is somewhat stronger than on PbS-2H (see Table S2 for the adsorption energies). This would be another reason why KGF-9-2H is more catalytically active than PbS-2H. On KGF-9-2H, the S-H groups and CO_2 are aligned in height, while on PbS-2H, CO_2 is higher than the S-H groups. In the TS structure on PbS-2H, the S-H group that supplies H to CO_2 protrudes, and this structural distortion may be a reason for the higher activation barrier on PbS-2H than on KGF-9-2H. The results of the vibrational analysis for these TS structures are shown in the SI (Figure S11). An energy diagram of the entire reaction is shown in Figure S12 for a comprehensive analysis. A discussion of the rate-limiting step based on this is given in Supplementary Note 4 in the SI. Briefly, if we focus on the process from CO_2 adsorption to formic acid desorption, the desorption process appears to be the rate-limiting step. In addition to that, the inherent electron-hole recombination that occurs on the KGF-9 photocatalyst dominates the overall quantum yield of CO_2 photoreduction.

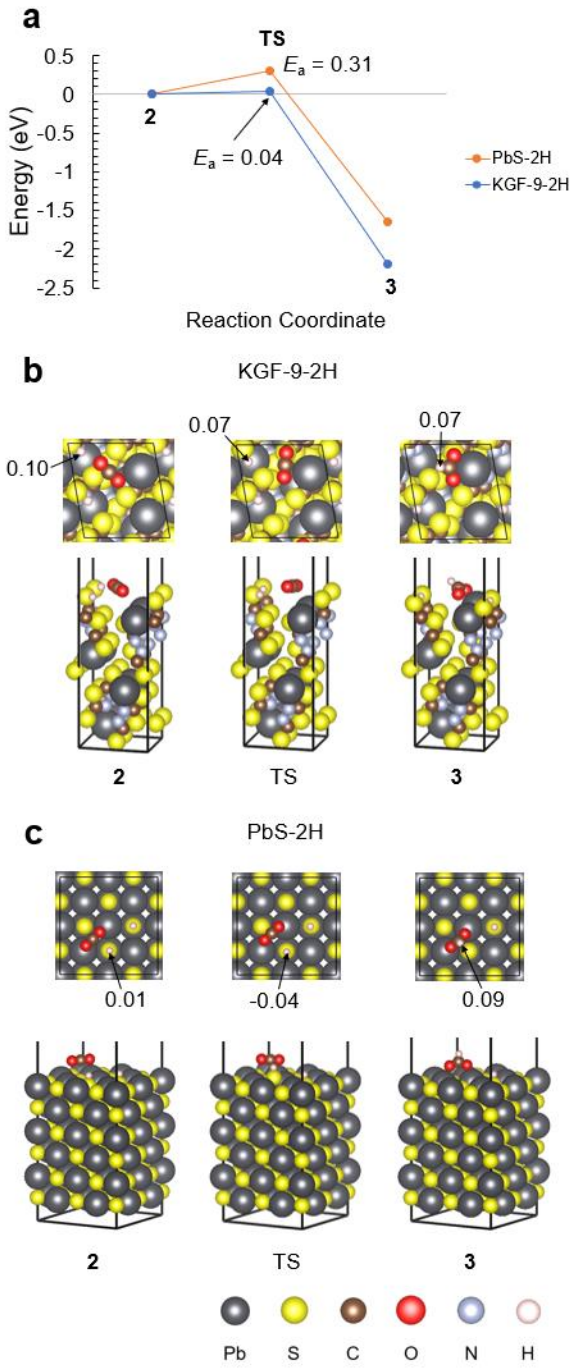

Figure 4. (a) Energy changes associated with the transition from state **2** to state **3** via the TS on the KGF-9-2H (blue line) and PbS-2H (orange line) surfaces and the structures of state **2**, TS, and state **3** for the (b) KGF-9-2H and (c) PbS-2H surfaces. The number near the arrow pointing to an H atom indicates its Bader charge.

The reaction we are considering here is quite simple: H moves from the S-H group to the C atom of CO_2. The state of H in this reaction is very interesting. Figures 4b and 4c show the calculated Bader charge of H at each step. Their absolute values are close to zero, indicating that H transfers as a hydrogen atom, not as a proton or hydride. It is interesting to note that in the FDH catalyst, H is thought to migrate as a hydride,[36,37,38] which is different from KGF-9.

It is clear that CO_2 on the KGF-9-2H surface undergoes a one-electron reduction by transferring an H atom to CO_2, but where does the second electron come from? To get a clue, we calculated the density of states (DOS) profile of the KGF-9-2H surface with CO_2 adsorbed (Figure 5a) and that of the non-reduced surface (Figure S13). The general shapes of the DOS profiles for both surfaces are similar. However, an important difference is that in the DOS of the KGF-9-2H surface, the Fermi level is very close to the CB. This suggests that KGF-9 is an n-type semiconductor and that the KGF-9-2H surface is reduced. Furthermore, it is clear that there are electrons occupying the states immediately below the Fermi level (indicated by the blue arrow), which correspond exactly to the electrons in the CB shown in Scheme 2. In other words, the second electron would come from there. In addition to the total DOS (TDOS), a partial DOS (PDOS) profile corresponding to the CO_2 portion is also plotted in Figure 5a. The sharp peak around E = 2.3 eV corresponds to the lowest unoccupied molecular orbital (LUMO) of CO_2. This is the orbital that will accept the electron. Similar features are seen in the DOS profile of the CO_2 adsorbed PbS-2H surface (Figure 5b).

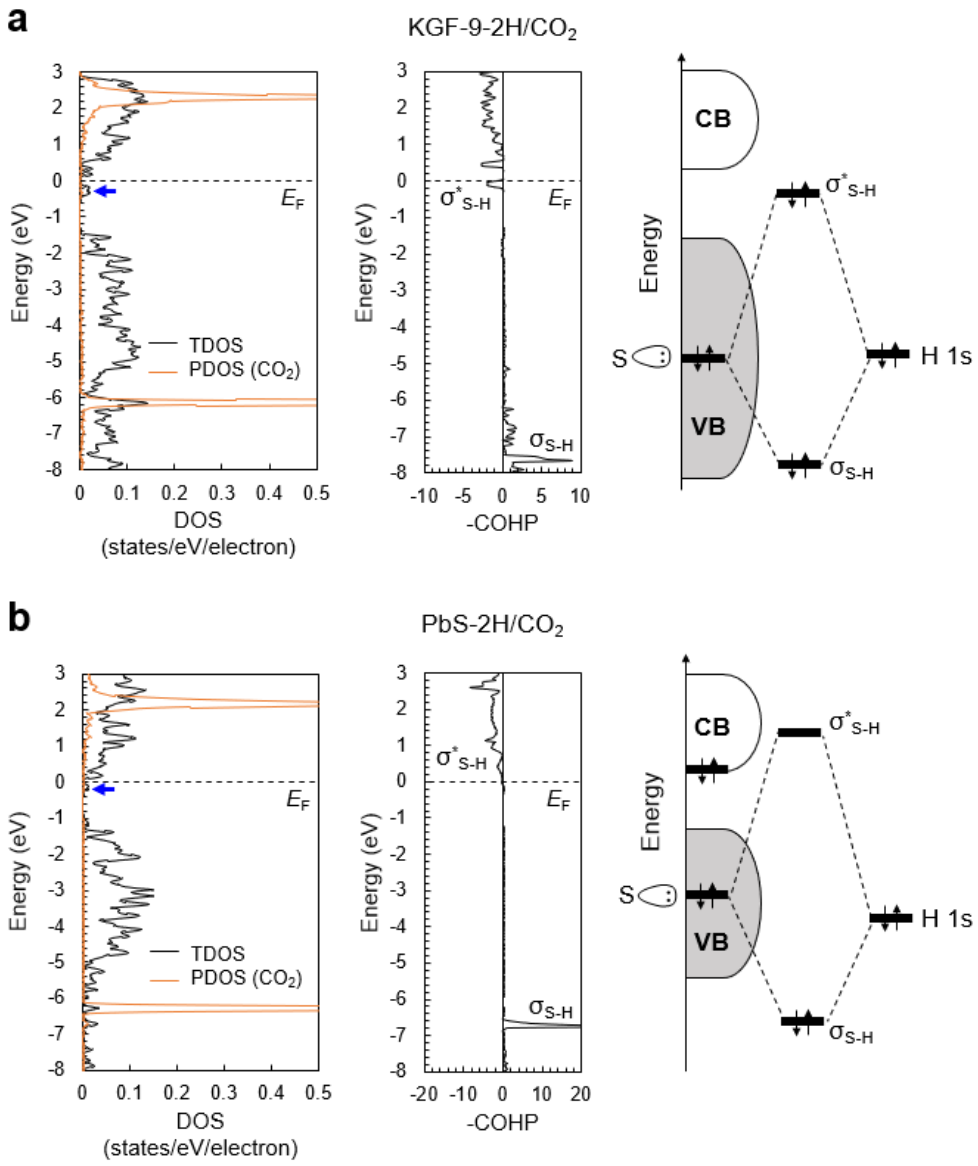

Figure 5. DOS profiles calculated for CO_2-adsorbed (a) KGF-9-2H and (b) PbS-2H surfaces (left), COHP profiles of the S-H bonds at these surfaces (middle), and schematic illustrations of the formation of the σ_{S-H} and σ^*_{S-H} orbitals by orbital interactions between an orbital corresponding to the lone pair of the S atom and the 1s orbital of H (right). Total DOS (TDOS) is indicated by the black line and the partial DOS (PDOS) for CO_2 is indicated by the orange line. The Fermi level (E_F) is indicated by the dashed line. The COHP values are multiplied by -1, so that positive values correspond to bonding interactions and negative values correspond to antibonding interactions.

Next to the DOS profile in Figure 5a, a COHP profile calculated for the S-H bonds of the KGF-9-2H surface is shown on the same energy scale. From this figure, it can be seen that there is a peak corresponding to the S-H antibonding orbital (σ^*_{S-H}) just below the Fermi level. COHP analysis was also performed for the S-H bonds on the PbS-2H surface, and its COHP profile is shown in Figure 5b, but there is no peak just below the Fermi level. On the PbS-2H surface, the second electron for CO_2 reduction likely originates from a source other than the S-H bond. This significant disparity in surface electronic structures between KGF-9-2H and PbS-2H is clearly shown by the schematic orbital interaction diagrams drawn on the basis of each COHP profile. They are shown next to the COHP profiles. These orbital interaction diagrams are drawn in the style established by the work of Hoffmann and co-workers.[42] We would like to add that the COHP profile for the S-H bond of FDH, calculated using a cluster model for its active center, is interestingly similar to that for the KGF-9-2H surface (Figure S14). That is, peaks for σ^*_{S-H} states are identified just below the Fermi level.

The orbital interaction diagram for the KGF-9-2H surface shows a two-orbital four-electron situation, while that for the PbS-2H surface shows a two-orbital two-electron situation. The former orbital interaction represents an unstable state,[27] and it would be difficult to produce that state thermally, but it would be possible photochemically. In the case of KGF-9, the energy of the σ^*_{S-H} orbital is lower than that of the CB minimum (CBM), so some of the excited electrons will flow out into the σ^*_{S-H} orbital. In the case of PbS, however, the energy of the σ^*_{S-H} orbital is higher than that of the CBM, so the excited electrons remain in the CB.

The electronic state at the surface is more or less delocalized compared to the molecular electronic state.[43] In the COHP diagram for KGF-9-2H, there is a peak corresponding to the σ^*_{S-H}

orbital just below the Fermi level, but not all states corresponding to the σ^*_{S-H} orbital are occupied because there are also antibonding peaks above the Fermi level. The SH bond on KGF-9-2H is likely to be weak, but not so weak that its formation is not expected. The weak nature of the bond may also contribute to the ease of hydrogen transfer from the SH group to CO_2.

The energy level ordering of the σ^*_{S-H} orbital and the CBM that produces the above differences is determined mainly by three factors: 1) The stronger S-H bonding on the PbS surface destabilizes its σ^*_{S-H} orbital. Indeed, the COBI calculated for the S-H bond on the PbS surface is 0.96, while that on the KGF-9 surface is 0.90. This probably reflects the fact that the S-H bonds on the KGF-9-2H surface are slightly longer than those on the PbS-2H surface; the enhanced strength of the S-H bonds on the PbS-2H surface may also involve a larger contribution from ionic bonding on the PbS-2H surface (see Supplementary Note 5 in the SI for more details). The difference in the strength of the S-H bond on these surfaces is also reflected as a difference in the adsorption energy of H_2 (see Supplementary Note 6 in the SI for more details). 2) PbS has a higher VB maximum (VBM) energy than KGF-9, further destabilizing its σ^*_{S-H} orbital (VBM levels calculated with respect to the vacuum level: KGF-9 -5.0 eV, PbS -4.5 eV), in agreement with experimental values.[9, 44] 3) PbS has a smaller band gap than KGF-9 and a lower CBM energy: The experimentally measured band gap of KGF-9 is about 2.5 eV[9] while that of PbS is about 0.4 eV.[45] The band gap of PbS is so small that it makes sense that it would not work as a photocatalyst because of its very low reducing and/or oxidizing ability of photogenerated carriers. PbS may not have a suitable band edge potential for CO_2 reduction and BIH oxidation. As described above, the S-H bond on the KGF-9 surface is unique. However, it would be possible to apply the concept of CO_2 activation by occupied antibonding σ orbitals on the catalyst surface to other bonds than S-H,

such as O-H bonds (see Supplementary Note 7 in the SI for more details). This would be supported by the fact that α-FeOOH catalyzes the reduction of CO_2 to formic acid.[46]

The charge densities corresponding to the states indicated by the blue arrows just below the Fermi levels in the DOS profiles of Figures 5a and 5b are shown in Figures 6a and 6b. They correspond to the square of the wave function of the energy interval in question (partial charge densities). Figure 6a shows that most states are localized near the surface, i.e., near CO_2. This is expected to result in effective electron injection into CO_2. One cannot find population on the S-H bond containing the H atom that will be transferred toward CO_2 in the CO_2 reduction reaction, but one can find it on the other S-H bond. We further analyzed it using a contour plot (see the inset in Figure 6a) and found that there is a point between the S and H atoms where the amplitude of the wave function becomes zero, i.e., a node of the wave function, so that the electronic state shown there is indeed derived from the σ^*_{S-H} orbital.

On the other hand, Figure 6b shows that the states are mainly localized inside the slab. This feature is also observed in a thicker slab model (see Figure S18), and this feature does not change even if the atomic coordinates of the lower layers of the slab model are fixed to those of the bulk (see Figure S19). Figure S20 shows the charge density distribution corresponding to the CBM of the non-reduced PbS surface, the location of which is in good agreement with that in Figure 6b. This confirms the correctness of the situation shown in the orbital interaction diagram in Figure 5b. These observations indicate that not only the proximity of the energy level of the supplied electrons to the LUMO energy level of CO_2, but also the spatial distribution of the wave function of the electrons is important for effective electron injection from the reduced catalyst surface to CO_2 to be achieved. These results clearly indicate the superiority of KGF-9 in CO_2 reduction.

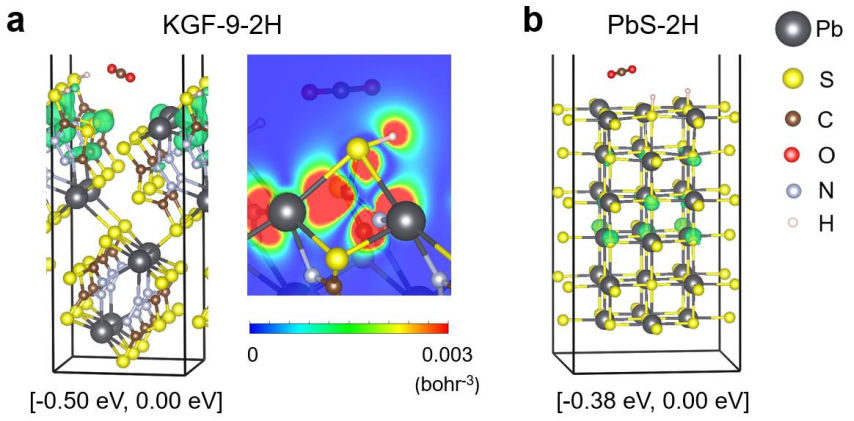

Figure 6. Isosurface plots of partial charge density calculated for the (a) KGF-9-2H and (b) PbS-2H surfaces. The energy interval used to calculate the partial charge density is shown below each plot. For KGF-9-2H, a contour plot of the partial charge density on a plane containing the S-H bond with population is also shown.

The change in Bader charge of each atom during the transition from state **2** to state **3** was also examined. The formate species was found to have a charge of -0.74 both on KGF-9 and on PbS. Atoms on the catalyst surface with more positive Bader charge differences (Δq) before and after the reaction are shown in Figure 7. Since the total Δq values shown in this figure are balanced by the negative charge of the formate species, we may conclude that the electron density is primarily supplied to CO_2 by these atoms. Note that it is the origin of the second electron that is being discussed here; the first electron has moved with the H atom. On the KGF-9-2H surface (Figure 7a), electron density is supplied not only from Pb but also from the organic ligand (tadt unit) in its vicinity. The degree of electron density reduction on the tadt unit is greater than that on Pb, suggesting that the tadt unit plays a more important role than Pb. This tadt unit is presumed to be the active center for CO_2 reduction on the KGF-9 surface. It should be added that the tadt unit

depicted here is different from that with the S-H group that provides the hydrogen atom to the CO_2 molecule. An analysis using a monomeric model of KGF-9 highlights the importance of the coexistence of the tadt unit and Pb in the catalytic reaction (see Supplementary Note 8 in the SI for more details). We would also like to add that in a previous study,[9] a comparison of the UV-vis spectra of KGF-9 and H_2tadt has already shown that the coordination of the H_2tadt ligand to Pb^{2+} has a decisive influence on the visible light absorption properties of KGF-9. Thus, the combination of the organic ligand and the metal center is deemed to be the source of the unique visible light-harvesting and CO_2 reduction properties of KGF-9. It may be possible to make other metallic elements, such as Sn, take on the role of Pb.[47] Theoretical studies on photocatalysis of CO_2 reduction with such Pb-free CPs remain a future challenge. On the other hand, the electron density supplied to CO_2 on the PbS-2H surface (Figure 7b) appears to be entirely derived from Pb atoms. At the topmost surface, the Pb atoms bonded to the oxygen atoms of the formate species show the largest Δq values. In addition, the electron density of the lower Pb atoms is also found to be reduced, although the absolute values of Δq are not as large.

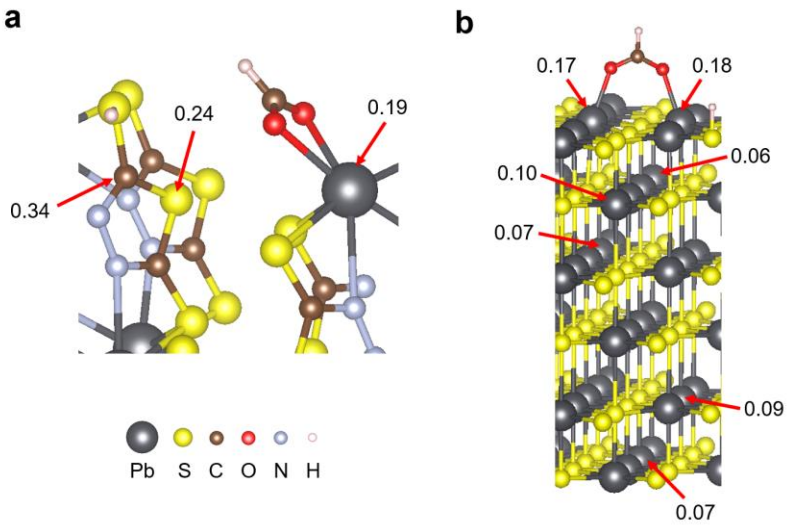

Figure 7. Atoms with more positive Bader charge changes (Δq) in the change from state **2** to state **3** calculated for the (a) KGF-9-2H and (b) PbS-2H surfaces are indicated. Atoms with indicated Δq values were selected in descending order of Δq until the total Δq value was balanced by the negative charge of the formate species.

Comparing Figure 6a and Figure 7a, one can see that the positions of the atoms with large charge changes and those with large partial charge density values roughly coincide, localized on the surface. This is because these electronic states are derived from the formation of the S-H bond at the surface, as discussed in Figure 5a. On the other hand, comparing Figure 6b and Figure 7b, one can see that the positions of the atoms with large charge changes and those with large partial charge density values do not coincide. This means that on the PbS surface, the second electron supplied to CO_2 does not necessarily come from the highest occupied state.

In addition to the unique catalytic activity of KGF-9, the high selectivity of KGF-9 was also investigated. In addition to the two-electron reduction pathway from CO_2 to formic acid, there is also a two-electron reduction pathway to carbon monoxide (see Scheme 5).[48,49] As we have discussed throughout this paper, if an $HCOO^-$ intermediate is produced, it would be converted to

formic acid. On the other hand, if a $COOH^-$ intermediate is formed, it would be converted to CO and H_2O. Thus, it is suggested that the difference in stability of the $HCOO^-$ and $COOH^-$ intermediates is the key to discussing the selectivity of this reaction.

Scheme 5. Schematic Mechanisms for the Two-Proton/Two-Electron ($2H^+/2e^-$) CO_2 Reduction Reactions to HCOOH and CO.[a]

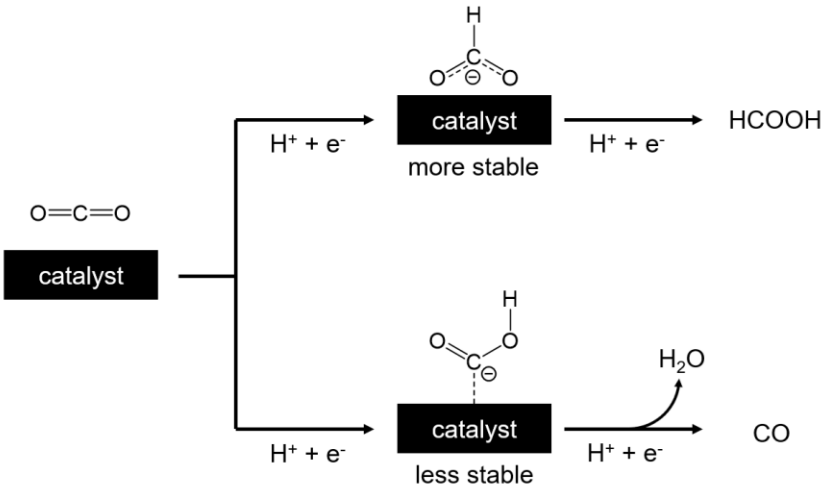

[a] Comparing the energies of the adsorption states of $HCOO^-$ (top) and $COOH^-$ (bottom), $HCOO^-$ is more stable on the KGF-9 surface. See text for details.

If CO_2 were to be converted to $COOH^-$ on the KGF-9-2H surface, how $COOH^-$ would be adsorbed is shown in Figure S22. The energy of such a structure was found to be about 1.1 eV higher than the energy of the adsorbed structure of $HCOO^-$. Since the $HCOO^-$ adsorbed state is overwhelmingly more stable on the KGF-9 surface than the $COOH^-$ adsorbed state, $HCOO^-$ is expected to be formed with very high selectivity. The less stable adsorption of $COOH^-$ compared to $HCOO^-$ can be attributed to the energy difference between the two adsorbates themselves, with $COOH^-$ being 1.98 eV less stable than $HCOO^-$ at the B3LYP/6-31G(d) level. For $COOH^-$ to be

more stable than $HCOO^-$ on the surface, the interaction between the Pb atom and the C atom (seen in the adsorption structure of $COOH^-$) would have to be about 2 eV stronger than the interaction between the Pb atoms and the O atoms (seen in the adsorption structure of $HCOO^-$). Such a situation would be realized if elements with a strong affinity for C, such as Ni and Fe,[50] were used as active centers.

From the MO point of view, the instability of $COOH^-$ compared to $HCOO^-$ is explained by the interaction between the MOs of CO_2 and the 1s orbital of H. In $HCOO^-$, the 1s orbital has a large orbital overlap with the LUMO of CO_2 in a bonding manner, so the highest occupied molecular orbital (HOMO) thus formed is sufficiently stabilized (Figure 8a), while the HOMO of $COOH^-$ is hardly stabilized due to the smaller orbital overlap (Figure 8b). This is evident from the HOMO distribution, where $HCOO^-$, in contrast to $COOH^-$, has a large wave function amplitude around the H atom.

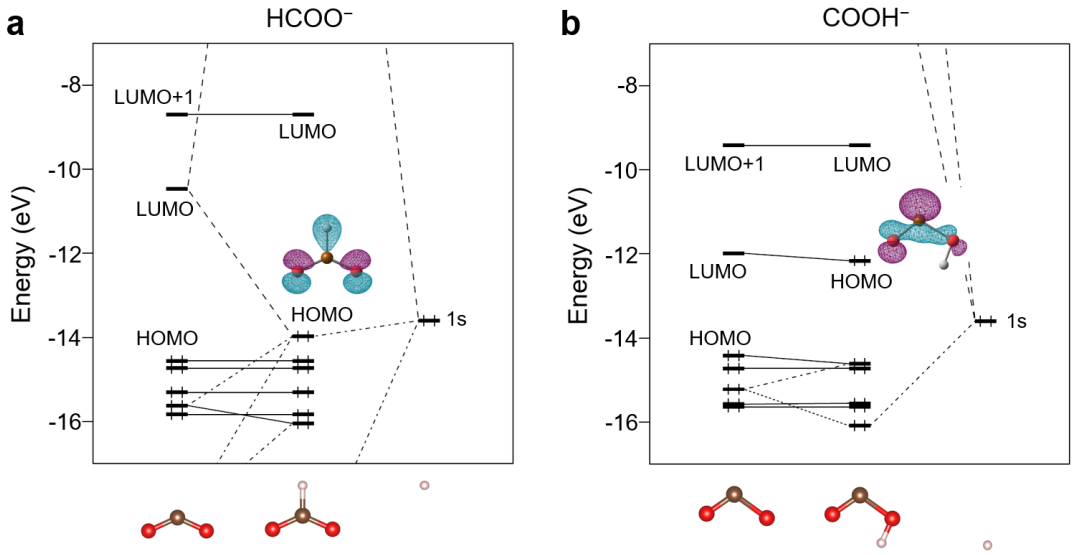

Figure 8. Interaction of the MOs of a bent CO_2 molecule with the 1s orbital of H to form the MOs of (a) $HCOO^-$ and (b) $COOH^-$. The HOMO distributions of $HCOO^-$ and $COOH^-$ are shown.

Conclusions

In this study, we have investigated the reduction of CO_2 to $HCOO^-$ by KGF-9, a recently developed visible-light responsive photocatalyst composed of a CP with Pb-S bonds. By contrast, PbS, a classical compound with Pb-S bonds, is known to have no photocatalytic activity for CO_2 reduction. We conducted a theoretical study to compare the difference in catalytic activity between them using periodic DFT calculations, finding that KGF-9 has a convex and concave surface, and that CO_2 adsorption is effective when CO_2 completely fits into the concavities of the surface. On the other hand, the surface of PbS is flat and does not seem to be particularly effective in stabilizing CO_2 adsorption.

The surface of KGF-9 as a photocatalyst was modeled as a structure with two H atoms adsorbed per unit cell. On the KGF-9 surface reduced by the addition of hydrogen atoms, the electron density corresponding to electrons with energy just below the Fermi level is mainly distributed on the catalyst surface. It contributes to effective electron injection into the adsorbed CO_2. Furthermore, such electron density is distributed not only on the Pb atoms but also on the thiadiazole skeleton in the surface, suggesting that not only the redox ability of the Pb atoms but also the organic π-conjugated skeleton of CP is important for the photoreduction of CO_2. DOS calculations of the hydrogenated PbS surface suggested a similar electronic structure, but the electron density corresponding to the electronic states with energies just below the Fermi level is mainly distributed inside the PbS solid, suggesting that electron injection from the PbS surface to CO_2 is almost prohibited. Such a difference seems to be determined by the presence of electrons in the σ^*_{S-H} orbital of the S-H bond formed on the surface: on the KGF-9 surface, electrons are accommodated in the σ^*_{S-H} orbital, but not on the PbS surface. This difference is due to the difference in S-H bond strength, VBM energy level, and band gap between the KGF-9 and PbS surfaces. Consistent with

the above, the exothermicity of the reaction from CO_2 to $HCOO^-$ on the reduced KGF-9 surface is greater than that on the reduced PbS surface, and the reaction barrier for the reaction on the reduced KGF-9 surface is much smaller than that on the reduced PbS surface.

In addition to the unique catalytic activity of KGF-9, the high selectivity of KGF-9 was also investigated, and it was shown that the origin of the high selectivity of KGF-9 can be explained by the stability of the intermediates: $HCOO^-$ is definitely more stable than $COOH^-$, and the order of stability is the same even when these are adsorbed on the KGF-9 surface. The difference in stability between $HCOO^-$ and $COOH^-$ can be explained by the interaction between the MOs of bent CO_2 and the 1s orbital of H.

The results of this study suggest that the KGF-9 surface has morphological features suitable for adsorption and hydrogenation of CO_2, and that the S-H groups on its surface have electronic features suitable for electron injection into CO_2. This, in turn, implies that further improvement of activity will be realized if bulk properties (e.g., crystallinity, morphology, specific surface area and so on) of KGF-9 are improved. More concretely, as the original KGF-9 has a very small specific surface area (< 1 m^2 g^{-1}, based on nitrogen adsorption measurement), increasing the surface area by refining the preparation method appears to be a straightforward way toward activity improvement. More difficult but worthwhile challenges include modifying organic ligands and metal centers to improve their light absorption and CO_2 adsorption properties, as well as the efficiency of electron and hydrogen transfer from the surface to CO_2.

ASSOCIATED CONTENT

Supporting Information.

Comparison of experimental and calculated structures, validation of slab thickness in slab model, discussion on the reduction of the KGF-9 surface by BIH including photographs and diffuse reflectance spectra of KGF-9, consideration on hydrogenation of KGF-9 and PbS surfaces, investigation of various adsorption modes of CO_2 and $HCOO^-$, the effect of the reduced state of the surface on the hydrogenation of CO_2, effects of spin-orbit coupling, analysis of the entire reaction process from adsorption of CO_2 to desorption of HCOOH from the surface of KGF-9-2H, DOS profiles of non-reduced surfaces of KGF-9 and PbS, COHP profile for the S-H bond of FDH, comparison of chemical states of S atoms on the KGF-9 and PbS surfaces, energetics of catalyst surface hydrogenation by H_2 adsorption, interaction of OH groups with CO_2, partial charge density calculated for the surface of a thick PbS-2H slab model adsorbing CO_2, effect of fixing atomic coordinates on partial charge density, charge density distribution corresponding to the CBM of the PbS surface, analysis of CO_2 reduction using a monomeric model of KGF-9, adsorption structures of $COOH^-$ on KGF-9 and PbS, and coordinates of the optimized structures.

AUTHOR INFORMATION

Corresponding Authors

Yuta Tsuji – *Faculty of Engineering Sciences, Kyushu University, Kasuga, Fukuoka 816-8580, Japan;* orcid.org/0000-0003-4224-4532; Email: tsuji.yuta.955@m.kyushu-u.ac.jp

Daisuke Tanaka –*Department of Chemistry, School of Science, Kwansei Gakuin University, Sanda, Hyogo 669-1337, Japan;* orcid.org/0000-0002-7469-0265; Email: dtanaka@kwansei.ac.jp

Kazuhiko Maeda – *Department of Chemistry, School of Science, Tokyo Institute of Technology, Meguro-ku, Tokyo 152-8550, Japan; Living Systems Materialogy (LiSM) Research Group, International Research Frontiers Initiative (IRFI), Tokyo Institute of Technology, 4259 Nagatsuta-*

cho, Midori-ku, Yokohama, Kanagawa 226-8502, Japan; orcid.org/0000-0001-7245-8318; Email: maedak@chem.titech.ac.jp

Authors

Sayoko Yamamoto – *Faculty of Engineering Sciences, Kyushu University, Kasuga, Fukuoka 816-8580, Japan;* Email: yamamoto.sayoko.754@m.kyushu-u.ac.jp

Yoshinobu Kamakura – *Department of Chemistry, School of Science, Tokyo Institute of Technology, Meguro-ku, Tokyo 152-8550, Japan;* Email: yoshinobukamakura1114@gmail.com

Chomponoot Suppaso – *Department of Chemistry, School of Science, Tokyo Institute of Technology, Meguro-ku, Tokyo 152-8550, Japan;* Email: chomponoot.ss@gmail.com

Notes

The authors declare no competing financial interest.

ACKNOWLEDGMENT

This work was supported by KAKENHI grant (number JP21K04996) from the Japan Society for the Promotion of Science (JSPS). The authors are grateful for a JSPS Grant-in-Aid for Transformative Research Areas (A) "Supra-ceramics" (grant numbers JP22H05146, JP22H05148, and JP23H04637). The computations in this work were performed using the computer facilities at the Research Institute for Information Technology, Kyushu University, at the Supercomputer Center, the Institute for Solid State Physics, the University of Tokyo, and at Cyberscience Center, Tohoku University. K.M. acknowledges a support from the JST-CREST program (JPMJCR20R2).

REFERENCES

(1) Hornberger, L.-S.; Adams, F. Photocatalytic CO_2 Conversion Using Metal-Containing Coordination Polymers and Networks: Recent Developments in Material Design and Mechanistic Details. *Polymers* **2022**, *14*, 2778.

(2) Gao, W.-Y.; Chrzanowski, M.; Ma, S. Metal-Metalloporphyrin Frameworks: A Resurging Class of Functional Materials. *Chem. Soc. Rev.* **2014**, *43*, 5841–5866.

(3) Wang, J.-L.; Wang, C.; Lin, W. Metal–Organic Frameworks for Light Harvesting and Photocatalysis. *ACS Catal.* **2012**, *2*, 2630–2640.

(4) Santaclara, J. G.; Kapteijn, F.; Gascon, J.; van der Veen, M. A. Understanding Metal–Organic Frameworks for Photocatalytic Solar Fuel Production. *CrystEngComm* **2017**, *19*, 4118–4125.

(5) Zhang, H.; Liu, G.; Shi, L.; Liu, H.; Wang, T.; Ye, J. Engineering Coordination Polymers for Photocatalysis. *Nano Energy* **2016**, *22*, 149–168.

(6) Verma, P.; Singh, A.; Rahimi, F. A.; Sarkar, P.; Nath, S.; Pati, S. K.; Maji, T. K. Charge-Transfer Regulated Visible Light Driven Photocatalytic H_2 Production and CO_2 Reduction in Tetrathiafulvalene Based Coordination Polymer Gel. *Nat. Commun.* **2021**, *12*, 7313.

(7) Liu, Y.; Guo, J. H.; Dao, X. Y.; Zhang, X. D.; Zhao, Y.; Sun, W. Y. Coordination Polymers with a Pyridyl-Salen Ligand for Photocatalytic Carbon Dioxide Reduction. *Chem. Commun.* **2020**, *56*, 4110–4113.

(8) Verma, P.; Rahimi, F. A.; Samanta, D.; Kundu, A.; Dasgupta, J.; Maji, T. K. Visible-Light-Driven Photocatalytic CO_2 Reduction to CO/CH_4 Using a Metal–Organic "Soft" Coordination Polymer Gel. *Angew. Chem., Int. Ed.* **2022**, *61*, e202116094.

(9) Kamakura, Y.; Sakura, C.; Saeki, A.; Masaoka, S.; Fukui, A.; Kiriya, D.; Ogasawara, K.; Yoshikawa, H.; Tanaka, D. Photoconductive Coordination Polymer with a Lead-Sulfur Two-Dimensional Coordination Sheet Structure. *Inorg. Chem.* **2021**, *60*, 5436–5441.

(10) Kamakura, Y.; Yasuda, S.; Hosokawa, N.; Nishioka, S.; Hongo, S.; Yokoi, T.; Tanaka, D.; Maeda, K. Selective CO_2-to-Formate Conversion Driven by Visible Light over a Precious-Metal-Free Nonporous Coordination Polymer. *ACS Catal.* **2022**, *12*, 10172–10178.

(11) Kresse, G.; Furthmüller, J. Efficiency of Ab-Initio Total Energy Calculations for Metals and Semiconductors Using a Plane-Wave Basis Set. *Comput. Mater. Sci.* **1996**, *6*, 15–50.

(12) Kresse, G.; Furthmüller, J. Efficient Iterative Schemes for Ab Initio Total-Energy Calculations Using a Plane-Wave Basis Set. *Phys. Rev. B* **1996**, *54*, 11169–11186.

(13) Perdew, J. P.; Burke, K.; Ernzerhof, M. Generalized Gradient Approximation Made Simple. *Phys. Rev. Lett.* **1996**, *77*, 3865–3868.

(14) Kresse, G.; Joubert, D. From Ultrasoft Pseudopotentials to the Projector Augmented-Wave Method. *Phys. Rev. B* **1999**, *59*, 1758–1775.

(15) Grimme, S.; Ehrlich, S.; Goerigk, L. Effect of the Damping Function in Dispersion Corrected Density Functional Theory. *J. Comput. Chem.* **2011**, *32*, 1456–1465.

(16) Momma, K.; Izumi, F. VESTA 3 for Three-Dimensional Visualization of Crystal, Volumetric and Morphology Data. *J. Appl. Crystallogr.* **2011**, *44*, 1272–1276.

(17) Chen, J.; Chen, Y.; Long, X.; Li, Y. DFT Study of Coadsorption of Water and Oxygen on Galena (PbS) Surface: An Insight into the Oxidation Mechanism of Galena. *Appl. Surf. Sci.* **2017**, *420*, 714–719.

(18) Jung, Y.-K.; Butler, K. T.; Walsh, A. Halide Perovskite Heteroepitaxy: Bond Formation and Carrier Confinement at the PbS–$CsPbBr_3$ Interface. *J. Phys. Chem. C* **2017**, *121*, 27351– 27356.

(19) Henkelman, G.; Uberuaga, B. P.; Jónsson, H. A Climbing Image Nudged Elastic Band Method for Finding Saddle Points and Minimum Energy Paths. *J. Chem. Phys.* **2000**, *113*, 9901–9904.

(20) Henkelman, G.; Jónsson, H. Improved Tangent Estimate in the Nudged Elastic Band Method for Finding Minimum Energy Paths and Saddle Points. *J. Chem. Phys.* **2000**, *113*, 9978–9985.

(21) Dronskowski, R.; Bloechl, P. E. Crystal Orbital Hamilton Populations (COHP): Energy-Resolved Visualization of Chemical Bonding in Solids Based on Density-Functional Calculations. *J. Phys. Chem.* **1993**, *97*, 8617–8624.

(22) Deringer, V. L.; Tchougréeff, A. L.; Dronskowski, R. Crystal Orbital Hamilton Population (COHP) Analysis as Projected from Plane-Wave Basis Sets. *J. Phys. Chem. A* **2011**, *115*, 5461–5466.

(23) Müller, P. C.; Ertural, C.; Hempelmann, J.; Dronskowski, R. Crystal Orbital Bond Index: Covalent Bond Orders in Solids. *J. Phys. Chem. C* **2021**, *125*, 7959–7970.

(24) Bader, R. *Atoms in Molecules: A Quantum Theory*; Oxford University Press: New York, 1990.

(25) Tang, W.; Sanville, E.; Henkelman, G. A Grid-Based Bader Analysis Algorithm without Lattice Bias. *J. Phys.: Condens. Matter* **2009**, *21*, 084204.

(26) Frisch, M. J.; Trucks, G. W.; Schlegel, H. B.; Scuseria, G. E.; Robb, M. A.; Cheeseman, J. R.; Scalmani, G.; Barone, V.; Petersson, G. A.; Nakatsuji, H.; Li, X.; Caricato, M.; Marenich, A. V.; Bloino, J.; Janesko, B. G.; Gomperts, R.; Mennucci, B.; Hratchian, H. P.; Ortiz, J. V.; Izmaylov, A. F.; Sonnenberg, J. L.; Williams-Young, D.; Ding, F.; Lipparini, F.; Egidi, F.; Goings, J.; Peng, B.; Petrone, A.; Henderson, T.; Ranasinghe, D.; Zakrzewski, V. G.; Gao, J.; Rega, N.; Zheng, G.; Liang, W.; Hada, M.; Ehara, M.; Toyota, K.; Fukuda, R.; Hasegawa, J.;

Ishida, M.; Nakajima, T.; Honda, Y.; Kitao, O.; Nakai, H.; Vreven, T.; Throssell, K.; Montgomery, J. A., Jr.; Peralta, J. E.; Ogliaro, F.; Bearpark, M. J.; Heyd, J. J.; Brothers, E. N.; Kudin, K. N.; Staroverov, V. N.; Keith, T. A.; Kobayashi, R.; Normand, J.; Raghavachari, K.; Rendell, A. P.; Burant, J. C.; Iyengar, S. S.; Tomasi, J.; Cossi, M.; Millam, J. M.; Klene, M.; Adamo, C. R.; Cammi, R.; Ochterski, J. W.; Martin, R. L.; Morokuma, K.; Farkas, O.; Foresman, J. B.; Fox, D. J. Gaussian 16, revision C.01; Gaussian, Inc.: Wallingford, CT, 2016.

(27) Albright, T. A.; Burdett, J.; Whangbo, M.-H. *Orbital Interactions in Chemistry*, 2nd ed.; Wiley: Hoboken, NJ, 2013.

(28) Landrum, G. A.; Glassey, W. V. YAeHMOP: Yet Another extended Huckel Molecular Orbital Package, version 3.0; http://yaehmop.sourceforge.net/

(29) Kuriki, R.; Matsunaga, H.; Nakashima, T.; Wada, K.; Yamakata, A.; Ishitani, O.; Maeda, K. Nature-Inspired, Highly Durable CO_2 Reduction System Consisting of a Binuclear Ruthenium(II) Complex and an Organic Semiconductor Using Visible Light. *J. Am. Chem. Soc.* **2016**, *138*, 5159–5170.

(30) Rao, H.; Schmidt, L. C.; Bonin, J.; Robert, M. Visible-Light-Driven Methane Formation from CO_2 with a Molecular Iron Catalyst. *Nature* **2017**, *548*, 74–77.

(31) Wang, S. B.; Guan, B. Y.; Lu, Y.; Lou, X. W. Formation of Hierarchical In_2S_3-$CdIn_2S_4$ Heterostructured Nanotubes for Efficient and Stable Visible Light CO_2 Reduction. *J. Am. Chem. Soc.* **2017**, *139*, 17305–17308.

(32) Pellegrin, Y.; Odobel, F. Sacrificial Electron Donor Reagents for Solar Fuel Production. *C. R. Chim.* **2017**, *20*, 283–295.

(33) Wei, B.; Calatayud, M. The Subsurface Diffusion of Hydrogen on Rutile TiO_2 Surfaces: A Periodic DFT Study. *Top. Catal.* **2021**, *1*, 1–11.

(34) Di Valentin, C.; Pacchioni, G.; Selloni, A. Electronic Structure of Defect States in Hydroxylated and Reduced Rutile TiO_2 (110) Surfaces. *Phys. Rev. Lett.* **2006**, *97*, 166803.

(35) Tsuji, Y.; Hoffmann, R.; Miller, J. S. Revisiting $Ir(CO)_3Cl$. *Polyhedron* **2016**, *103*, 141–149.

(36) Maia, L. B.; Moura, I.; Moura, J. J. G. Carbon Dioxide Utilisation─The Formate Route. In *Enzymes for Solving Humankind's Problems*; Moura, J. J. G., Moura, I., Maia, L. B., Eds.; Springer International Publishing: Cham, 2021; pp 29–81.

(37) Maia, L. B.; Fonseca, L.; Moura, I.; Moura, J. J. Reduction of Carbon Dioxide by a Molybdenum-Containing Formate Dehydrogenase: A Kinetic and Mechanistic Study. *J. Am. Chem. Soc.* **2016**, *138*, 8834–8846.

(38) Niks, D.; Duvvuru, J.; Escalona, M.; Hille, R. Spectroscopic and Kinetic Properties of the Molybdenum-Containing, NAD^+-Dependent Formate Dehydrogenase from Ralstonia Eutropha. *J. Biol. Chem.* **2016**, *291*, 1162–1174.

(39) Maia, L. B.; Moura, J. J.; Moura, I. Molybdenum and Tungsten-Dependent Formate Dehydrogenases. *J. Biol. Inorg. Chem.* **2015**, *20*, 287–309.

(40) Österlund, L. Structure-Reactivity Relationships of Anatase and Rutile TiO_2 Nanocrystals Measured by In Situ Vibrational Spectroscopy. *Solid State Phenom.* **2010**, *162*, 203–219.

(41) Steiner, S.; Khmelevskyi, S.; Marsmann, M.; Kresse, G. Calculation of the magnetic anisotropy with projected-augmented-wave methodology and the case study of disordered $Fe_{1-x}Co_x$ alloys. *Phys. Rev. B* **2016**, *93*, 224425.

(42) Zheng, C.; Apeloig, Y.; Hoffmann, R. Bonding and Coupling of C1 Fragments on Metal Surfaces. *J. Am. Chem. Soc.* **1988**, *110*, 749–774.

(43) Hoffmann, R. *Solids and Surfaces: A Chemist's View of Bonding in Extended Structures*; VCH: New York, 1988.

(44) Yeon, D. H.; Lee, S. M.; Jo, Y. H.; Moon, J.; Cho, Y. S. Origin of the Enhanced Photovoltaic Characteristics of PbS Thin Film Solar Cells Processed at Near Room Temperature. *J. Mater. Chem. A* **2014**, *2*, 20112–20117.

(45) Li, X.-B.; Guo, P.; Zhang, Y.-N.; Peng, R.-F.; Zhang, H.; Liu, L.-M. High Carrier Mobility of Few-Layer PbX (X = S, Se, Te). *J. Mater. Chem. C* **2015**, *3*, 6284–6290.

(46) An, D.; Nishioka, S.; Yasuda, S.; Kanazawa, T.; Kamakura, Y.; Yokoi, T.; Nozawa, S.; Maeda, K. Alumina-Supported Alpha-Iron(III) Oxyhydroxide as a Recyclable Solid Catalyst for CO_2 Photoreduction under Visible Light. *Angew. Chem. Int. Ed.* **2022**, *61*, e202204948.

(47) Kamakura, Y.; Suppaso, C.; Yamamoto, I.; Mizuochi, R.; Asai, Y.; Motohashi, T.; Tanaka, D.; Maeda, K. Tin(II)-Based Metal–Organic Frameworks Enabling Efficient, Selective Reduction of CO_2 to Formate under Visible Light. *Angew. Chem. Int. Ed.* **2023**, *62*, e202305923.

(48) Zhao, S.; Li, S.; Guo, T.; Zhang, S.; Wang, J.; Wu, Y.; Chen, Y. Advances in Sn-Based Catalysts for Electrochemical CO_2 Reduction. *Nanomicro Lett.* **2019**, *11*, 1–19.

(49) Muthuperiyanayagam, A.; Nabi, A. G.; Zhao, Q.; Aman-ur-Rehman; Tommaso, D. D. Adsorption, Activation, and Conversion of Carbon Dioxide on Small Copper-Tin Nanoclusters. *Phys. Chem. Chem. Phys.* **2023**, *25*, 13429-13441.

(50) Hori, M.; Tsuji, Y.; Yoshizawa, K. Bonding of C_1 Fragments on Metal Nanoclusters: A Search for Methane Conversion Catalysts with Swarm Intelligence. *Phys. Chem. Chem. Phys.* **2021**, *23*, 14004–14015.